RSC Applied Interfaces

ROYAL SOCIETY OF CHEMISTRY

PAPER

View Article Online
View Journal | View Issue

Cite this: *RSC Appl. Interfaces*, 2024, **1**, 1166

MOF-based sensors for the detection of airborne α-pinene†

P. Pires Conti,[ab] P. Iacomi,[ac] P. F. Brântuas,[a] M. Nicolas,[b] R. Anton,[b] S. Moularat,[b] S. Dasgupta,[d] N. Steunou,[d] G. Maurin[a] and S. Devautour-Vinot*[a]

Two metal–organic frameworks, DUT-4(Al) and MIL-100(Fe), were explored as sensitive layers deposited at the surface of QCM transducers for the detection of α-pinene, a terpenic volatile organic compound encountered in indoor air at a trace level. Both sensors displayed sensitive, fast, reversible and repeatable response toward exposure to α-pinene, in complementary ranges of contaminant concentration: DUT-4(Al)@QCM was demonstrated to be attractive for the detection of α-pinene at 0.5 ppm $< C_{\alpha\text{-pinene}} <$ 4.8 ppm, while MIL-100(Fe)@QCM was found more efficient at $C_{\alpha\text{-pinene}} >$ 4.8 ppm. As an alternative to using two complementary QCM sensors, a single device prepared by coating the QCM by mixing DUT-4(Al) and MIL-100(Fe) was envisaged. Interestingly, DUT-4(Al)/MIL-100(Fe)@QCM benefited from a synergistic effect of both MOFs: it showed high sensitivity for detecting α-pinene in a wider range of concentration than that explored with sensors based on a single MOF, without losing the high level of sensor performances, in terms of response time, reversibility and repeatability.

Received 23rd January 2024,
Accepted 29th April 2024

DOI: 10.1039/d4lf00027g

rsc.li/RSCApplInter

Introduction

Indoor air pollution has become a major concern in developed countries due to the increased time people spend in closed environments, including homes, transportation, public buildings, and workplaces. Human exposure to low-quality air causes various adverse health effects associated with respiratory illnesses, allergies, neurological dysfunctions, and even cancerous diseases.[1,2] Predominant indoor air pollutants encompass particulate matter, toxic inorganic gas and volatile organic compounds (VOCs), including terpenes.[3–5] Terpenes are chemicals derived from isoprene $(C_5H_8)_n$. They are biogenic volatile organic compounds (BVOCs), a key constituent of essential oils produced through secondary metabolic pathways in plants.[6] Accordingly, they are mainly used as fundamental fragrance or flavouring agents in cosmetics and cleaning products, in the agri-food industry, as well as additives in aromatherapy.[7–9] Their emission in indoor air leads to concentration levels that greatly vary according to human usage and activity, typically falling within the range of 0.01 to 6000.00 μg m^{-3}.[3,8,10] Airborne terpene levels in the wood industry, *e.g.* sawmill and joinery related activities, are even higher and fluctuate from 1000 to 250 000 μg m^{-3}.[11–14] The impact of terpenes on human health is paradoxical: their inhalation, even at low concentration, can adversely lead to headaches or allergic reactions, while some of them have shown medicinal and therapeutic benefits on pathogenic diseases and some cancers.[15,16] However, most importantly, the primary concern associated with airborne terpenes relies on their ability to form harmful by-products upon reacting with oxidizing agents like ozone (O_3), hydroxyl radicals ($OH^{\bullet}$), and nitrate radicals ($NODVS_3^{\bullet}$).[8,17] These by-products, including formaldehyde, acetic acid, or ultrafine particles, are more hazardous to health than the original terpene precursors. To prevent this effect, it is thus crucial to mitigate terpene emission which also calls for a drastic monitoring of the pollutant concentration in indoor/industrial environments using sensors.

The quantification of VOCs is achieved using various analytical tools. Generally, an aliquot of air is collected, pre-concentrated, and further analysed by gas chromatography (GC) coupled with different types of detectors such as a flame ionisation detector (FID), a photoionization detector (PID) or a mass spectrometer (MS).[18–21] These devices show many advantages in terms of detection limit, accuracy and selectivity, but are doubly inconvenient since they require skilled staff to perform complex operations and most importantly they cannot achieve real-time/temporal data

[a] *UMR 5253 – CNRS/UM/ENSCM, Pole Chimie Balard Recherche, Institut Charles Gerhardt Montpellier (ICGM), 34293 Montpellier Cedex 5, France. E-mail: sabine.devautour-vinot@umontpellier.fr*
[b] *Centre Scientifique et Technique du Bâtiment (CSTB), 24 Rue Joseph Fournier, 38400 Saint-Martin-d'Hères, France*
[c] *Surface Measurement Systems (SMS), Unit 5, Wharfside, London HAO 4PE, UK*
[d] *Institut Lavoisier de Versailles (ILV), UMR 8180, Université Paris Saclay, Université de Versailles St Quentin en Yvelines, 78035 Versailles Cedex, France*
† Electronic supplementary information (ESI) available. See DOI: https://doi.org/10.1039/d4lf00027g

resolution.[18] Likewise, portable and micro GC-based devices are solutions that still show some limitations in terms of cost, size/weight, and resolution time.[22,23] As an alternative, miniaturized electronic devices, based on optical, electrical, or mass sensitive transducers, are favourable solutions to provide continuous and online monitoring of airborne contaminants with high sensitivity and durability.[24,25] Propitiously, these devices are very attractive when combined with a coated sensitive layer: the transducer displays universal applicability, portability, robustness, and fast response, while the sensing material is a key factor in determining and amplifying the sensitivity and the selectivity of the device.[26,27] Accordingly, many efforts have been dedicated for designing sensing films, which associate numerous active sites exposed to the analyte with good mechanical properties and device flexibility.[28,29] In this context, metal oxides,[30] polymers,[30,31] carbon-based materials,[30,32] zeolites,[33] macrocyclic molecules,[34] and porous coordination polymers as pure components or combined in composites[18,35–39] have been considered for the detection of a large variety of VOCs. By contrast, only a handful of these materials were investigated for the sensing of terpenes. Apart from two optical sensors using self-assembled Au nanoparticles[40] and one type of covalent organic framework,[41] most of the efforts have been prioritized on the incorporation of molecularly imprinted polymers (MIPs) to electrical and gravimetric-based sensors.[42–49] As the main advantage, MIPs offer selective recognition of a molecule at a low interference level due to memory effects through binding sites with tailored size, shape, and functionality complementary to the target molecular pollutant. However, they require laborious preparation and face upscaling issues in terms of extra cost and manufacturing restrictions, which still limits their transfer at the industrial level.[50]

Interestingly, metal–organic frameworks (MOFs) have recently emerged as alternative sensitive sorbents incorporated in various sensor devices.[18,36,51,52] MOFs are constructed through an almost infinite combination of metal ions/clusters and organic polydentate ligands, resulting in an almost limitless variety of structures with regular porosity, a wide range of pore sizes, and multivariate functionalities.[51,53] Benefiting from the advantages of MOFs, *e.g.*, their unique and tuneable structural/chemical features, combined with their processability to form films, MOF-based sensors have been successfully designed, covering a large panel of devices, including resistive-, capacitive-, optical-, magnetic- and resonant-based sensors.[36,51,54,55] Although MOF sensors have been reported for the detection of various toxic gases and a myriad of VOCs,[36,55–57] we are aware of only rare examples for the detection of terpenes so far.[58,59] Herein, a series of MOFs were deposited on quartz crystal microbalance (QCM) supports to design gravimetric-based sensors for the detection of α-pinene, identified as one of the most abundant terpenes in nature and in indoor environments.[60,61] Typically, two well-known MOFs, whose pores are accessible to α-pinene (kinetic diameter = 7 Å), *i.e.* DUT-4(Al) and MIL-100(Fe), were considered. DUT-4(Al), DUT = Dresden University of Technology, is a microporous MOF, resulting from the combination of aluminum clusters coordinated to 2,6-naphthalenedicarboxylate (ndc) ligands generating rhombic-shaped channels about 8.5 × 8.5 Å in dimensions,[62] while MIL-100(Fe), MIL = Materials of Institute Lavoisier, is a mesoporous MOF built from iron trimeric octahedral clusters and carboxylate moieties (benzene-1,3,5-tricarboxylate (BTC)), exhibiting pentagonal and hexagonal cages of 25 Å and 29 Å diameters, accessible through windows of 6 Å and 9 Å, respectively.[63] Both MOFs can be synthesized through cost-effective and environmentally friendly protocols and therefore have gained significant attention in adsorption-related fields, including gas storage[64–67] and VOC sensing applications.[68,69] The sensing performances of DUT-4(Al)@QCM and MIL-100(Fe)@QCM toward α-pinene were discussed in terms of sensitivity, reversibility, the range of concentration covered, limit of detection, and response/recovery times. As a further step, a mixed DUT-4(Al)/MIL-100(Fe)@QCM device was prepared: it showed attractive sensing performance compared to those displayed by the sensors constructed with the single MOFs.

Experimental

Materials

α-Pinene (98% purity) was purchased from Sigma-Aldrich. Ethanol suspension of DUT-4(Al) (7 g L^{-1}) was purchased from Materials Center, Dresden.[62] To synthesize MIL-100(Fe), $Fe(NO_3)_3{\cdot}9H_2O$ and trimesic acid were purchased from Alfa Aesar and Sigma Aldrich respectively and they were used without any further purification. Powdered MOFs were obtained by drying the ethanolic suspensions at 353 K for 3 h. 10 MHz AT-cut QCMs with Cr/Au electrodes were purchased from QuartzPro.

MIL-100(Fe) nanoparticles were synthesized at room temperature by dissolving 0.72 g (1.78 mmol) of $Fe(NO_3)_3{\cdot}9H_2O$ and 0.25 g (1.19 mmol) of trimesic acid in 70 mL of distilled water according to the previously reported protocol.[70] The yield of MIL-100(Fe) was close to 79%. The reaction mixture was stirred at room temperature for 48 h. The synthesized MOF was washed with water and absolute ethanol. The MOF nanoparticles were stored as a colloidal suspension in absolute ethanol (11.5 g L^{-1}). After preparation, the suspension was sonicated in an ultrasonic bath for 2 h.

Characterization methods

Powder X-Ray diffraction (PXRD) data were collected on a Panalytical X'Pert PRO PXRD diffractometer, using a Cu Kα radiation source (λ_α = 1.54184 Å) in the Bragg–Brentano reflection geometry. The samples (powdered MOFs and MOF@QCM) were placed in a spinning sample holder with a low-background silicon insert. The PXRD pattern of the pristine powdered MIL-100(Fe) was collected on a Bruker D8 diffractometer in a range of 2θ from 2 to 15°. The infrared spectrum of MIL-100(Fe) was recorded on an FTIR Magna

550 Nicolet spectrophotometer with a diamond tip at a resolution of 4 cm^{-1}. The thermal stability of MIL-100(Fe) was analyzed on a thermogravimetric analyzer, Model Perkin Elmer SDA 6000, by heating the sample up to 700 °C with a heating rate of 3 °C min^{-1} under an oxygen atmosphere. The N_2 sorption isotherms of the powdered MOFs were measured at 77 K using a Micromeritics Tristar II Plus. Dynamic light scattering (DLS) experiments were carried out on the ethanolic suspension using Malvern Zetasizer Nano ZS apparatus equipped with a He–Ne laser operating at a wavelength of 633 nm and a detection angle of 173° (back scattering). Scanning electron microscopy (SEM) images of the powdered MOF and MOF@QCM devices were acquired using an FEI Quanta 200 FEG microscope, operating at 30 kV in high vacuum mode with gold sputtered samples. Energy-dispersive X-ray (EDX) analysis was performed using a silicon drift detector (SDD) (Ultim Max 100 mm^2 Oxford Instruments) combined with the SEM equipment.

MOF@QCM preparation

MIL-100(Fe)@QCM and DUT-4(Al)@QCM were prepared by drop-casting 15 μL of the ethanol suspension of DUT-4(Al) (7.0 g L^{-1}) and MIL-100(Fe) (11.5 g L^{-1}) on the QCM surface, then the suspensions were sonicated for 2 h before deposition. The films were dried at room temperature (298 K) for 24 h. The DUT-4(Al)/MIL-100(Fe) suspension was prepared by mixing 50 μL of each individual suspension (DUT-4(Al): 7.0 g L^{-1} and MIL-100(Fe): 11.5 g L^{-1}). The mixture was sonicated for 2 h before being used. 15 μL of the suspension was drop-casted on the QCM surface and further dried at room temperature for 24 h.

α-Pinene sorption

Sorption isotherms of α-pinene were acquired at 303 K using in-house modified DVS vacuum apparatus from Surface Measurement Systems, in the concentration range of 0.01 to 950 ppm for the powders and 0.05 to 715 ppm for MOF@QCMs.[71] An argon/α-pinene flow was entrained by a vacuum system over a stainless-steel sample pan and a QCM holder placed in the reference side of the apparatus, allowing the recording of both the gravimetric sorption isotherm on powder and sensor response on QCM. Pressure control was achieved using a butterfly valve located before the outlet. The saturation degree of α-pinene in the gas carrier was evaluated using a calibration procedure detailed in the ESI† (Fig. S1). The powder sample and the MOF@QCM sensor were *in situ* activated under vacuum (10^{-7} Bar) at 423 K for 2 h.

Gravimetric measurements on MOFs as powder

About 10–15 mg of the MIL-100(Fe) or DUT-4(Al) powder was introduced in a stainless-steel sample pan. The powder mass change was evaluated using a symmetrical microbalance with a resolution of ±0.1 μg.

Sensor response on MOF@QCM

The MOF-based sensor was introduced in a home-made holder and inserted inside the DVS apparatus. The QCM holder was connected through BNC cables to a Rohde&Schwartz ZNC3 vector analyzer. The QCM resonance frequency was measured from 9.8 MHz to 10.1 MHz, with 100 ms resolution and frequency sweeps at 1 s resolution. Experiments were replicated three times for DUT-4(Al)@QCM and MIL-100(Fe)@QCM and twice for DUT-4(Al)/MIL-100(Fe) @QCM. Data treatment was processed using Python.

Results and discussion

Prior to collecting the response of the MOF-based sensors, gravimetric sorption isotherms of α-pinene with the powdered MOFs were obtained at 303 K to demonstrate the ability of DUT-4(Al) and MIL-100(Fe) to adsorb α-pinene in a concentration range, comprising terpene contamination levels encountered in common indoor environments ([0.05–1.08] ppm, *i.e.* [270–6000.00] μg m^{-3})[3,8,10] and at the industrial level ([0.2–45.0] ppm, *i.e.* [1000–250 000] μg m^{-3}), in the typical cases of sawmill and joinery related activities.[11–14] Dried DUT-4(Al) and MIL-100(Fe) powders, whose crystallinity and purity were checked by PXRD, and textural properties verified by N_2 sorption experiments (see Fig. S2–S7,† for details), were introduced in the home-modified DVS apparatus. Fig. 1a and b show that the sorption profiles are standard type-I for both solids. Interestingly, a few but not negligible amount of α-pinene is adsorbed at a very low concentration, *i.e.*, $C_{\alpha\text{-pinene}} < 1$ ppm. With increasing α-pinene concentration, the sorption capacity increases steeply, while the uptake at saturation for MIL-100(Fe), *i.e.*, 0.40 g g^{-1} at 350 ppm, is slightly concentration up-shifted compared to that recorded for DUT-4(Al), *i.e.*, 0.37 g g^{-1} at 250 ppm. Interestingly, both sorption processes are reversible under vacuum, combined with a small and even negligible hysteresis loop between the adsorption and desorption branches for DUT-4(Al) and MIL-100(Fe), respectively. Accordingly, both onset and removal of α-pinene indoors are expected to be tracked by these MOFs, supporting their applicability as sensitive layers incorporated in sensors for the detection of α-pinene traces. The difference

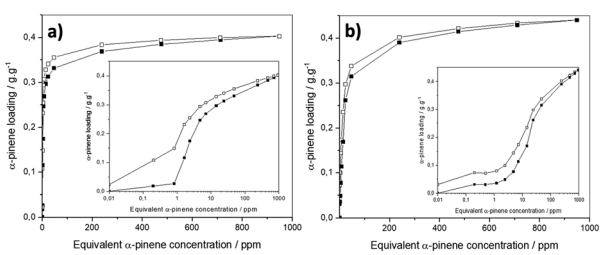

Fig. 1 Gravimetric sorption isotherms of α-pinene recorded at 303 K on a) DUT-4(Al) and b) MIL-100(Fe) powder, increasing (filled black squares) and decreasing (empty black squares) α-pinene concentration. Insets show the isotherms on a semi-logarithmic basis. Lines are guides for the eyes.

in S_{BET} and V_{pore} determined from N_2 sorption measurements recorded before and after α-pinene sorption is negligible (*cf.* Fig. S3, S7, and Table S1†), evidencing that the α-pinene sorption process can be seen as reversible for DUT-4(Al) and MIL- 100(Fe). Noteworthily, this is in contrast with MIL-125(Ti)-NH_2, whose irreversible sorption profile makes it suitable for α-pinene capture but inappropriate for sensing applications.[71]

Based on the above-mentioned sorption behaviours of DUT-4(Al) and MIL-100(Fe) towards α-pinene, these MOFs were incorporated in mass-detecting QCM devices. As described in the experimental section, DUT-4(Al)@QCM and MIL-100(Fe)@QCM sensors were prepared by drop-casting the MOF colloidal suspensions on the QCM surface. The mean aggregate hydrodynamic diameters for both DUT-4(Al) and MIL-100(Fe) suspensions were determined through DLS analysis. They fall within 200 nm, in agreement with the small size of the agglomerates of MIL-100(Fe) and DUT-4(Al), evidenced from the SEM images collected on the powdered MOFs (Fig. S8 and S9†). According to the PXRD patterns shown in Fig. S10 and S12,† the characteristic Bragg peaks of DUT-4(Al) and MIL-100(Fe) are observed for the respective MOF@QCMs, stating that the structural integrity of the pristine MOFs is maintained over the shaping process. In addition, the SEM images show that both films are homogeneously deposited on the whole surface of the quartz supports, with film thicknesses around 2.85 μm and 1.21 μm for DUT-4(Al)@QCM and MIL-100(Fe)@QCM, respectively (Fig. S11 and S13†).

The responses of DUT-4(Al)@QCM and MIL-100(Fe)@QCM *versus* α-pinene concentration are depicted in Fig. 2a and b, respectively. The operation principle of QCM technology is based on the resonant frequency shift of the quartz crystal (Δf), induced by minute mass fluctuations of the sensor surface (Δm), due to interactions between the analyte (α-pinene) and the sensitive layer (DUT-4(Al) or MIL-100(Fe))[25] that functions as an adsorptive surface. According to the Sauerbrey equation (see eqn (1)),[72] Δf is directly proportional to Δm induced by α-pinene adsorption in the MOF layer:

$$\Delta f = \frac{-2f_0^{\,2}}{A\sqrt{\rho_q \mu_q}}\Delta m \quad (1)$$

where $\Delta f = f - f_0$ and f and f_0 correspond to the resonance frequency of the MOF@QCM device recorded at fixed α-pinene concentration $C_{\alpha\text{-pinene}}$ and at $C_{\alpha\text{-pinene}} = 0.05$ ppm, respectively. In eqn (1), A is the QCM surface area and μ_q and ρ_q are the shear modulus and the density of the device, respectively.[73] In Fig. 2a and b, DUT-4(Al)@QCM and MIL-100(Fe)@QCM response is compared with the gravimetric sorption isotherm recorded on each powder MOF. The sensor response fairly follows the α-pinene gravimetric sorption profile in the entire concentration range, demonstrating that the MOF-sensitive layer is responsible for the sensor signal. This is consistent with the flat and negligible response recorded on the blank QCM (grey triangles in Fig. 2a and b). In addition, the sensor response shows negligible deviation over cycling, stating that data are repeatable over three consecutive cycles of α-pinene sorption (see Fig. S14a–S14d). Importantly, cycling experiments do not impact the structural integrity of both MOF@QCM films, as evidenced by similar PXRD patterns recorded before and after α-pinene sorption experiments (*cf.* Fig. S10 and S12†). DUT-4(Al)@QCM and MIL-100(Fe)@QCM are thus able to detect α-pinene in a sharp and reversible manner, along with full regenerability, good repeatability, and satisfactory stability.

The kinetic response of DUT-4(Al)@QCM and MIL-100(Fe)@QCM was collected in the time domain, while the sensors were exposed to sudden changes of α-pinene concentrations from 2 ppm to 5 ppm, 24 ppm, or 47 ppm and *vice versa* (*cf.* Fig. 3a–d). During the concentration increase steps, the time-dependence of the sensor response closely matches with the dead time of the apparatus to reach the target concentration value, evidencing a very fast response time although it cannot

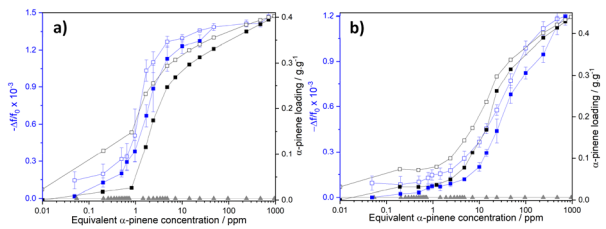

Fig. 2 Relative frequency shift for a) DUT-4(Al)@CM and b) MIL-100(Fe)@QCM *versus* increasing (filled blue square) and decreasing (empty blue square) α-pinene concentration. The blank experiment recorded on an uncoated QCM is illustrated by grey triangles. Error bars represent the standard deviation over 3 cycles. Gravimetric sorption isotherms of α-pinene with DUT-4(Al) and MIL-100(Fe) powders are displayed by filled and empty black squares for the adsorption and desorption branches, respectively. Lines are guides for the eyes.

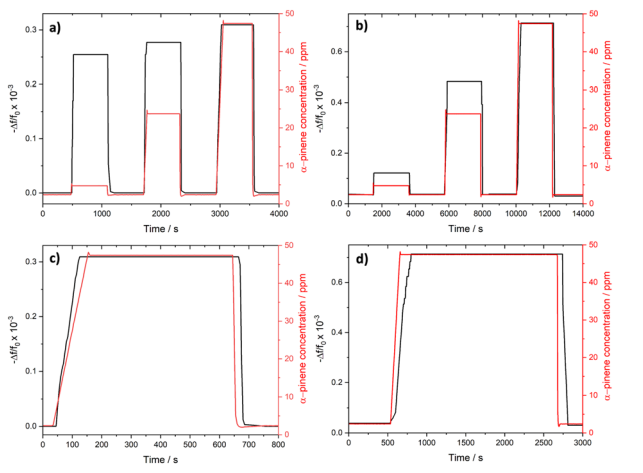

Fig. 3 Real-time sensor response of a) DUT-4(Al)@QCM and b) MIL-100(Fe)@QCM to multiple changes of α-pinene concentration from 2 ppm to 5 ppm, 24 ppm, and 47 ppm and *vice versa*, with a highlight of the kinetics of the last cycle (2 ppm–47 ppm–2 ppm) for c) DUT-4(Al)@QCM and d) MIL-100(Fe)@QCM.

be assessed. When decreasing the α-pinene concentration toward 2 ppm, Δf consistently returns back to its baseline value in a few dozen seconds (see Table S2†). While recovery times are shorter for DUT-4(Al)@QCM (20–28 s) than for MIL-100(Fe)@QCM (51–70 s), both sensors provide kinetic performances in line with the requirements for real-time estimation of the contamination of enclosed places by airborne terpenes.

The sensor sensitivity, S, was estimated by evaluating the slope of the relative frequency shift *versus* the α-pinene concentration (*cf.* Fig. S15 and Table S3†). Both devices display complementary behaviours in distinct α-pinene concentration ranges, making DUT-4(Al)@QCM and MIL-100(Fe)@QCM effective for sensing terpenes in indoor air and industrial environments, respectively. DUT-4(Al)@QCM is very sensitive ($S = 1 \times 10^{-3}$ $\log_{10}(\text{ppm})^{-1}$) to $C_{\alpha\text{-pinene}}$ ranging from 1 to 4.8 ppm. By contrast, MIL-100(Fe)@QCM is unresponsive for $C_{\alpha\text{-pinene}} < 4.8$ ppm, and shows a better sensitivity ($S = 5 \times 10^{-4}$ $\log_{10}(\text{ppm})^{-1}$) than DUT-4(Al)@QCM for $C_{\alpha\text{-pinene}} \geq 4.8$ ppm ($S = 2 \times 10^{-4}$ $\log_{10}(\text{ppm})^{-1}$). The concentration range in which DUT-4(Al)@QCM is very sensitive to α-pinene is down-shifted compared to that for MIL-100(Fe)@QCM, in line with the fact that $C_{\alpha\text{-pinene}}$ at which the gravimetric sorption uptake starts to be significant is 10 times lower for DUT-4(Al) (~1 ppm) than for MIL-100(Fe) (~10 ppm). The higher α-pinene affinity of DUT-4(Al) is related to the beneficial size matching effect between the guest molecule (α-pinene kinetic diameter = 7 Å) and the pore channel of DUT-4 (8 × 8 Å). In contrast, the mesopores of MIL-100(Fe) (cage diameters = 25 Å and 29 Å) are too large to enable an optimum confinement for α-pinene. Interestingly, coupling both MOF-based sensors should enable the detection of minute changes in α-pinene concentration over a wide range.

To take advantage of the complementary nature of the two mass-sensing films without using two standalone QCM sensors, we elected to prepare a unique DUT-4(Al)/MIL-100(Fe)@QCM device. For this purpose, the DUT-4(Al) and MIL-100(Fe) colloidal solutions were mixed together, resulting in a single mixed component suspension, further drop-casted on a QCM support (*cf.* methodology section). The PXRD pattern collected on the film includes typical signatures of both DUT-4(Al) and MIL-100(Fe) structures (*cf.* Fig. S16†). The SEM images evidenced that the film of DUT-4(Al)/MIL-100(Fe)@QCM is crack-free (thickness ≈ 9.9 μm, *cf.* Fig. S17a and S17b†), and EDX analysis demonstrated that Al and Fe elements are homogenously distributed (Fig. S17c†).

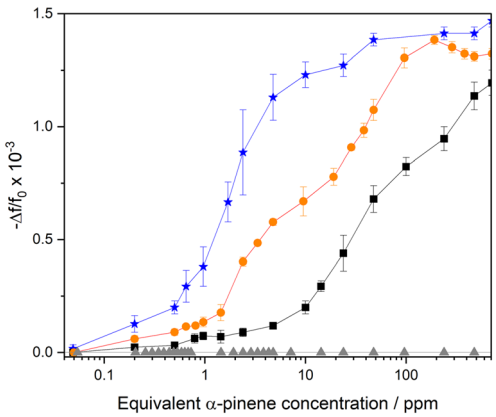

Fig. 4 Relative frequency shift for DUT-4(Al)/MIL-100(Fe)@QCM (orange circles), DUT-4(Al)@QCM (blue stars), MIL-100(Fe)@QCM (black squares), and uncoated QCM (grey triangles) *versus* increasing α-pinene concentration. Error bars represent the standard deviations over cycling experiments. Lines are guides for the eyes.

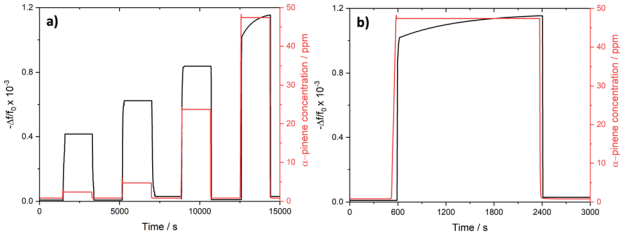

Fig. 5 a) Real-time sensor response of DUT-4(Al)/MIL-100(Fe)@QCM to multiple changes of α-pinene concentration from 0.8 ppm to 2 ppm, 5 ppm, 24 ppm, and 47 ppm and *vice versa*, b) with a highlight of the kinetics of the last cycle (0.8 ppm–47 ppm–0.8 ppm).

The comparison of the frequency response for DUT-4(Al)/MIL-100(Fe)@QCM, DUT-4(Al)@QCM, MIL-100(Fe)@QCM, and uncoated QCM *versus* α-pinene concentration is depicted in Fig. 4. The response of DUT-4(Al)/MIL-100(Fe)@QCM is in between that of pure phase based sensors, *i.e.* DUT-4(Al)@QCM and MIL-100(Fe)@QCM, evidencing that it results from a combination of both MOFs components. Most importantly, it shows high sensitivity ($S = 6 \times 10^{-4}$ $\log_{10}(\text{ppm})^{-1}$) for $C_{\alpha\text{-pinene}}$ varying from 0.6 ppm to 100 ppm, *i.e.*, the concentration range of interest for the detection of this contaminant in both indoor air and industry settings. In addition, the sensor response of DUT-4(Al)/MIL-100(Fe)@QCM is repeatable (*cf.* Fig. S18a and S18b†), and the structural integrity of the DUT-4(Al)/MIL-100(Fe) film is maintained after α-pinene sorption, as evidenced by similar PXRD patterns collected on the device before and after recording the sensor response toward α-pinene exposure (*cf.* Fig. S16†).

The response time of DUT-4(Al)/MIL-100(Fe)@QCM with respect to α-pinene concentration changes is depicted in Fig. 5. The signal follows the α-pinene concentration switch, with the recovery time varying from 95 s to 120 s according to the starting concentration level of α-pinene. While slightly longer than what was observed on the pure phase MOF-based sensors, it still satisfies the prerequisite for monitoring α-pinene contamination on site.

Conclusions

Two MOFs, DUT-4(Al) and MIL-100(Fe), were explored for detecting traces of airborne α-pinene. The MOFs were selected according to their sorption profiles toward α-pinene,

showing good guest affinity at low concentration, a reversible process associated with the absence or a negligible hysteresis loop. Both MOFs were successfully integrated into QCM transducers and subsequently tested in a wide range of α-pinene vapor concentration. The corresponding sensors display a fast, reversible and repeatable response, in good correspondence with their sorption isotherms. DUT-4(Al) @QCM shows high sensitivity at low α-pinene concentration (ranging from 0.6 to 4.8 ppm). In contrast, MIL-100(Fe) @QCM displays higher sensitivity for concentrations exceeding 4.8 ppm. This prompted us to create a new QCM device, combining both MOFs. The resulting DUT-4(Al)/MIL-100(Fe)@QCM demonstrated a linear response with the logarithm of α-pinene concentration and high sensitivity over a concentration range (0.6 to 100 ppm) wider than that achieved by sensors based on single MOFs. The sensor maintains the good repeatability and rapid recovery time seen in single components. Decisively, this work reports an unprecedented design of an effective α-pinene sensor combining two MOF components, which opens new perspectives to mitigate pollution of volatile terpenes in indoor and wood-related industry environments. This strategy paves the way towards new horizons to gas/vapor sensor technology, wherein complementary components are synergistically associated in the sensing layer to widen the sensitivity range. Incorporated in an electronic nose, this innovative approach may offer an alternative route for the response tuning to better address cross-sensitivity and selectivity with high accuracy.[74–76] Further adjustments are still required for improving the MOF@QCM sensor robustness and selectivity over water. The coating of the MOF-film external surface with hydrophobic polymers is envisioned as a promising solution to attain this objective.[77–79]

Author contributions

Conceptualization: PPC and SDV. Synthesis and characterization of MIL-100(Fe): SD and NS. Film preparation and characterization, adsorption and sensing investigation, and data analysis: PPC, PI, PFB and SDV. Writing – original draft: PPC, SDV and GM. Writing – review and editing: all authors. Supervision: SDV.

Conflicts of interest

There are no conflicts to declare.

Acknowledgements

We thank Région Occitanie (MADE and IDEE project) and Centre Scientifique et Technique du Bâtiment (CSTB) for financial support. PXRD experiments were performed with the support of the Balard Plateforme d'Analyses et de Caractérisation (PAC Balard). The authors would like to acknowledge Frédéric Fernandez from the MEA platform, Université de Montpellier, for the SEM-EDX experiments. This work was supported by the Ecole Universitaire de recherche PSGS HCH Humanities, Creation, Heritage, Investissement d'Avenir ANR-17-EURE-0021 - Fondation des sciences du patrimoine. NS and SD thank Noëlle Timbart and Agnès Lattuati-Derieux (Centre de Recherche et de Restauration des Musées de France, Paris) for fruitful discussion, as well as Bruno Berini (GEMAC, University of Versailles St Quentin en Yvelines) for the characterization of films.

References

1 K. E. Paleologos, M. Y. E. Selim and A. O. Mohamed, Indoor air quality: pollutants health effects, and regulations, in *Pollution Assessment for Sustainable Practices in Applied Sciences and Engineering*, ed. A.-M. O. Mohamed, E. K. Paleologos and F. M. Howari, Butterworth-Heinemann, 2021, pp. 405–489.
2 S. Vardoulakis, E. Giagloglou, S. Steinle, A. Davis, A. Sleeuwenhoek, K. S. Galea, K. Dixon and J. O. Crawford, *Int. J. Environ. Res. Public Health*, 2020, **17**, 8972.
3 S. Angulo Milhem, M. Verriele, M. Nicolas and F. Thevenet, *Environ. Sci. Pollut. Res.*, 2020, **27**, 14365.
4 S. Rovelli, A. Cattaneo, A. Fazio, A. Spinazzè, F. Borghi, D. Campagnolo, C. Dossi and D. M. Cavallo, *Atmosphere*, 2019, **10**, 57.
5 C. Shrubsole, S. Dimitroulopoulou, K. Foxall, B. Gadeberg and A. Doutsi, *Build. Environ.*, 2019, **165**, 106382.
6 Y. Lin, X. Lun, W. Tang, Z. Zhang, X. Jing, C. Fan and Q. Wang, *For. Ecosyst.*, 2021, **8**, 52.
7 S. Angulo Milhem, M. Verriele, M. Nicolas and F. Thevenet, *Atmos. Environ.*, 2021, **246**, 118060.
8 S. Angulo-Milhem, M. Verriele, M. Nicolas and F. Thevenet, *Atmos. Environ.*, 2021, **244**, 117863.
9 T. Kim, B. Song, K. S. Cho and I. S. Lee, *Int. J. Mol. Sci.*, 2020, **21**, 2187.
10 B. C. Singer, H. Destaillats, A. T. Hodgson and W. W. Nazaroff, *Indoor Air*, 2006, **16**, 179.
11 A. Straumfors, R. Olsen, H. L. Daae, A. Afanou, D. McLean, M. Corbin, A. Mannetje, B. Ulvestad, B. Bakke, H. L. Johnsen, J. Douwes and W. Eduard, *Ann. Work Exposures Health*, 2018, **62**, 674.
12 K. A. Eriksson, N. L. Stjernberg, J. O. Levin, U. Hammarström and M. C. Ledin, *Scand. J. Work, Environ. Health*, 1996, **22**, 182.
13 C. Rosenberg, A. Ruonakangas, T. Liukkonen, I. Welling and P. Jäppinen, *Am. J. Ind. Med.*, 1999, **36**, 149.
14 U. Svedberg and B. Galle, *Appl. Occup. Environ. Hyg.*, 2000, **15**, 686.
15 D. Cox-Georgian, N. Ramadoss, C. Dona and C. Basu, Therapeutic and Medicinal Uses of terpenes, in *Medicinal Plants*, ed. N. Joshee, S. Dhekney and P. Parajuli, Springer, Cham, 2019, pp. 333–359.
16 J. Pereira, M. Miguel Castro, F. Santos, A. Rita Jesus, A. Paiva, F. Oliveira and A. R. C. Duarte, *Eur. J. Pharm. Biopharm.*, 2022, **175**, 13.
17 P. Wolkoff, *Int. J. Hyg. Environ. Health*, 2020, **225**, 113439.

18 S. M. Majhi, A. Ali, P. Rai, Y. E. Greish, A. Alzamly, S. G. Surya, N. Qamhieh and S. T. Mahmoud, *Nanoscale Adv.*, 2022, **4**, 697.
19 M. Woollam, M. Teli, P. Angarita-Rivera, S. Liu, A. P. Siegel, H. Yokota and M. Agarwal, *Sci. Rep.*, 2019, **9**, 2526.
20 X. Pang, W. Li, S. Wang, Z. Wu, S. Sun, Y. Lyu, D. Chen and H. Li, *J. Chromatogr. A*, 2023, **1704**, 464089.
21 S. Jin, L. Zhong, X. Zhang, X. Li, B. Li and X. Fang, *Int. J. Environ. Res. Public Health*, 2023, **20**, 5829.
22 R. Sharma, M. Zhou, M. D. Hunter and X. Fan, *J. Agric. Food Chem.*, 2019, **67**, 7530.
23 R. Epping and M. Koch, *Molecules*, 2023, **28**, 1598.
24 M. Khatib and H. Haick, *ACS Nano*, 2022, **16**, 7080.
25 C. K. McGinn, Z. A. Lamport and I. Kymissis, *ACS Sens.*, 2020, **5**, 1514.
26 S. Dhall, B. R. Mehta, A. K. Tyagi and K. Sood, *Sensor. Int.*, 2021, **2**, 100116.
27 M. Khatib and H. Haick, *ACS Nano*, 2022, **16**, 7080.
28 S. T. Han, H. Peng, Q. Sun, S. Venkatesh, K. S. Chung, S. C. Lau, Y. Zhou and V. A. L. Roy, *Adv. Mater.*, 2017, **29**, 1700375.
29 H. Jiang, L. Zheng, Z. Liu and X. Wang, *InfoMat*, 2020, **2**, 1077.
30 M. Tomić, M. Šetka, L. Vojkůvka and S. Vallejos, *Nanomater.*, 2021, **11**, 552.
31 Y. Yan, G. Yang, J. L. Xu, M. Zhang, C. C. Kuo and S. D. Wang, *Sci. Technol. Adv. Mater.*, 2020, **462**, 214517.
32 F. Yin, W. Yue, Y. Li, S. Gao, C. Zhang, H. Kan, H. Niu, W. Wang and Y. Guo, *Carbon*, 2021, **180**, 274.
33 G. T. M. Kadja, N. T. U. Culsum, S. Mardiana, N. J. Azhari, A. T. N. Fajar and Irkham, *Mater. Today Commun.*, 2022, **33**, 104331.
34 B. Phillips, S. Banerjee, X. Tu and L. Fang, *Supramol. Chem.*, 2020, **32**, 165.
35 T. Skorjanc, D. Shetty and M. Valant, *ACS Sens.*, 2021, **6**, 1461.
36 Y. Shen, A. Tissot and C. Serre, *Chem. Sci.*, 2022, **13**, 13978.
37 V. Gargiulo, M. Alfè, L. Giordano and S. Lettieri, *Chemosensors*, 2022, **10**, 290.
38 H. Wei, H. Zhang, B. Song, K. Yuan, H. Xiao, Y. Cao and Q. Cao, *Int. J. Environ. Res. Public Health*, 2023, **20**, 4388.
39 S. Wang, H. Li, H. Huang, X. Cao, X. Chen and D. Cao, *Chem. Soc. Rev.*, 2022, **51**, 2031.
40 B. Chen, C. Liu, M. Watanabe and K. Hayashi, *IEEE Sens. J.*, 2013, **13**, 4212.
41 X. Wu, X. Han, Q. Xu, Y. Liu, C. Yuan, S. Yang, Y. Liu, J. Jiang and Y. Cui, *J. Am. Chem. Soc.*, 2019, **141**, 7081.
42 F. L. Dickert, P. A. Lieberzeit, P. Achatz, C. Palfinger, M. Fassnauer, E. Schmid, W. Werther and G. Horner, *Analyst*, 2004, **129**, 432.
43 N. A. Humairah, F. Fadlunisa, K. A. Histhiningtyas, I. A. Fatyadi, R. Roto, A. Kusumaatmaja and K. Triyana, *Key Eng. Mater.*, 2020, **840**, 418.
44 C. J. Percival, S. Stanley, M. Galle, A. Braithwaite, M. I. Newton, G. McHale and W. Hayes, *Anal. Chem.*, 2001, **73**, 4225.
45 H. F. Hawari, N. M. Samsudin, M. N. Ahmad, A. Y. Md Shakaff, S. A. Ghani, Y. Wahab and U. Hashim, *Proceedings of the Third International Conference on Intelligent Systems Modelling and Simulation*, Kota Kinabalu, Malaysia, 2012, p. 723.
46 H. F. Hawari, S. M. Saad, N. M. Samsudin, A. Y. Md Shakaff, Y. Wahab and U. Hashim, IEEE International Conference on Circuits and Systems, 2013, p. 146.
47 S. P. Lee, *IOP Conf. Ser.: Mater. Sci. Eng.*, 2015, **87**, 012065.
48 L. Shang, C. Liu, B. Chen and K. Hayashi, *ACS Sens.*, 2018, **3**, 1531.
49 B. Chen, C. Liu, L. Ge and K. Hayashi, *Sens. Actuators, B*, 2016, **231**, 787.
50 Y. Hua, Y. Ahmadi and K. H. Kim, *Environ. Pollut.*, 2022, **311**, 119931.
51 Y. M. Jo, Y. K. Jo, J. H. Lee, H. W. Jang, I. S. Hwang and D. J. Yoo, *Adv. Mater.*, 2023, **35**, 2206842.
52 J. F. Olorunyomi, S. T. Geh, R. A. Caruso and C. M. Doherty, *Mater. Horiz.*, 2021, **8**, 2387.
53 M. H. Yap, K. L. Fow and G. Z. Chen, *Green Energy Environ.*, 2017, **2**, 218.
54 M. D. Allendorf, R. Dong, X. Feng, S. Kaskel, D. Matoga and V. Stavila, *Chem. Rev.*, 2020, **120**, 8581.
55 H. Y. Li, S. N. Zhao, S. Q. Zang and J. Li, *Chem. Soc. Rev.*, 2020, **49**, 6364.
56 A. M. Eagleton, M. Ko, R. M. Stolz, N. Vereshchuk, Z. Meng, L. Mendecki, A. M. Levenson, C. Huang, K. C. Macveagh, A. Mahdavi-Shakib, J. J. Mahle, G. W. Peterson, B. G. Frederick and K. A. Mirica, *J. Am. Chem. Soc.*, 2022, **144**, 23297.
57 M. Ko, A. Aykanat, M. K. Smith and K. A. Mirica, *Sensors*, 2017, **17**, 2192.
58 S. Okur, Z. Zhang, M. Sarheed, P. Nick, U. Lemmer and L. Heinke, *Sens. Actuators, B*, 2020, **306**, 127502.
59 Y. Liu, L. Liu, X. Chen, Y. Liu, Y. Han and Y. Cui, *J. Am. Chem. Soc.*, 2021, **143**, 3509.
60 S. Waidyanatha, M. Hackett, S. R. Black, M. D. Stout, T. R. Fennell, M. R. Silinski, S. L. Watson, J. Licause, V. G. Robinson, B. Sparrow, R. A. Fernando, S. Cooper and C. V. Rider, *Toxicol. Appl. Pharmacol.*, 2021, **418**, 115496.
61 Y. Noma and Y. Asakawa, Biotransformation of Monoterpenoids, in *Comprehensive Natural Products II: Chemistry and Biology: Development & Modification of Bioactivity*, ed. L. Mander and L. Hung-Wen, 2010, pp. 669–801.
62 I. Senkovska, F. Hoffmann, M. Fröba, J. Getzschmann, W. Böhlmann and S. Kaskel, *Microporous Mesoporous Mater.*, 2009, **122**, 93.
63 P. Horcajada, S. Surblé, C. Serre, D. Y. Hong, Y. K. Seo, J. S. Chang, J. M. Grenèche, I. Margiolaki and G. Férey, *Chem. Commun.*, 2007, 2820.
64 L. Mei, T. Jiang, X. Zhou, Y. Li, H. Wang and Z. Li, *Chem. Eng. J.*, 2017, **321**, 600.
65 B. Yuan, X. Wang, X. Zhou, J. Xiao and Z. Li, *Chem. Eng. J.*, 2019, **355**, 679.
66 G. B. Wang, K. Leus, K. Hendrickx, J. Wieme, H. Depauw, Y. Y. Liu, V. Van Speybroeck and P. Van Der Voort, *Dalton Trans.*, 2017, **46**, 14356.

67 X. Qian, R. Zhang, L. Chen, Y. Lei and A. Xu, *ACS Sustainable Chem. Eng.*, 2019, **7**, 16007.
68 J. H. Fu, Z. Zhong, D. Xie, Y. J. Guo, D. X. Kong, Z. X. Zhao, Z. X. Zhao and M. Li, *Angew. Chem., Int. Ed.*, 2020, **59**, 20489.
69 E. Gulcay-Ozcan, P. Iacomi, G. Rioland, G. Maurin and S. Devautour-Vinot, *ACS Appl. Mater. Interfaces*, 2022, **14**, 53777.
70 H. Zhao, S. Sene, A. M. Mielcarek, S. Miraux, N. Menguy, D. Ihiawakrim, O. Ersen, C. Péchoux, N. Guillou, J. Scola, J. M. Grenèche, F. Nouar, S. Mura, F. Carn, F. Gazeau, E. Dumas, C. Serre and N. Steunou, *J. Mater. Chem. B*, 2023, **11**, 3195.
71 P. P. Conti, K. Batra, P. Iacomi, C. V. Soares, S. Dasgupta, N. Steunou, A. Lattuati-Derieux, N. Timbart, M. Nicolas, R. Anton, S. Moularat, G. Maurin and S. Devautour-Vinot, *Chem. Commun.*, 2023, **59**, 7064.
72 X. Huang, Q. Bai, J. Hu and D. Hou, *Sensors*, 2017, **17**, 1785.
73 C. Zhang, S. Kaluvan, H. Zhang, G. Wang and L. Zuo, *Measurement*, 2018, **124**, 286.
74 W. Hu, L. Wan, Y. Jian, C. Ren, K. Jin, X. Su, X. Bai, H. Haick, M. Yao and W. Wu, *Adv. Mater. Technol.*, 2019, **4**, 1800488.
75 P. Qin, S. Okur, Y. Jiang and L. Heinke, *J. Mater. Chem. A*, 2022, **10**, 25347.
76 S. Acharyya, B. Jana, S. Nag, G. Saha and P. K. Guha, *Sens. Actuators, B*, 2020, **321**, 128484.
77 L. H. Mohd Azmi, P. Cherukupally, E. Hunter-Sellars, B. P. Ladewig and D. R. Williams, *Chem. Eng. J.*, 2022, **429**, 132304.
78 X. Qian, R. Zhang, L. Chen, Y. Lei and A. Xu, *ACS Sustainable Chem. Eng.*, 2019, **7**, 16007.
79 W. Zhang, Y. Hu, J. Ge, H. L. Jiang and S. H. Yu, *J. Am. Chem. Soc.*, 2014, **136**, 16978.